Acta Crystallographica Section B
Structural Science
ISSN 0108-7681

Structure determination of the $[Fe(teec)_6](BF_4)_2$ metal complex from laboratory and synchrotron X-ray powder diffraction data with grid-search techniques

Eva Dova,[a]* Arno F. Stassen,[b] René A. J. Driessen,[a] Ed Sonneveld,[a] Kees Goubitz,[a] René Peschar,[a] Jaap G. Haasnoot,[b] Jan Reedijk[b] and Henk Schenk[a]

[a]Laboratory for Crystallography, Institute of Molecular Chemistry, Universiteit van Amsterdam, Nieuwe Achtergracht 166, 1018 WV Amsterdam, The Netherlands, and [b]Leiden Institute of Chemistry, Gorlaeus Laboratories, Leiden University, PO Box 9502, 2300 RA Leiden, The Netherlands

Correspondence e-mail: eva@science.uva.nl

Received 9 April 2001
Accepted 16 May 2001

The structure of the coordination compound $[Fe(teec)_6](BF_4)_2$, hexa[1-(2-chloroethyl)tetrazole]iron(II) di(borotetrafluoride), has been determined using the grid-search techniques of the program suite *MRIA*. A Guinier-camera data set was used to determine the unit cell, the space group and to position the initial model. A high-resolution synchrotron powder data set was used to position a more detailed model using torsion-angle variation and to refine the structure leading to $Rp = 0.0689$, $Rw = 0.0805$ and $GoF = 1.38$. The crystal structure at room temperature shows the existence of two symmetry-equivalent iron(II) ions in the high-spin state.

1. Introduction

The grid-search techniques (Chernyshev & Schenk, 1998) continue to give successful results in solving structures from (high-resolution) powder diffraction data (Helmholdt *et al.*, 1998; Goubitz *et al.*, 1999, 2001; van Langevelde *et al.*, 1999). This paper presents another structure solved in this way. As has already been reported numerous times in the literature (Giacovazzo, 1996; Louër, 1998; McCusker *et al.*, 1999), the most severe problem in solving structures from powder data is extracting accurate intensities for use in the same techniques as developed for single-crystal diffraction data, such as direct methods and Patterson techniques. However, the larger the unit-cell volume the more difficult it is to extract accurate intensity values for each reflection and this problem becomes even more serious at higher Bragg angles where reflections heavily overlap, in the case of lower symmetry with higher reflection density and when the preferred orientation is present. High-resolution data, *e.g.* collected at a synchrotron radiation facility, are in general preferable but they do not ensure the solution of this problem. Many attempts have been made in the field of the accurate extraction of intensities (Toraya, 1986; Jansen *et al.*, 1992*a*,*b*, 1993; Cheary & Coelho, 1992) and much improvement has been gained. However, in the above-indicated cases the intensity extraction remains a major weak point in the structure determination procedure. Taking this into account, grid-search techniques, which are based on a direct handling of the molecular fragments in direct space, have some definite advantages because they do not require the intensity extraction of all individual reflections of the diffraction pattern and can handle groups of overlapping peaks. Moreover, experience shows that to locate an initial structural model a very large number of intensities is not necessary and, in general, only the low-angle part of a diffraction pattern, which suffers less from reflection overlap, is needed to extract intensity values.

However, care must be taken whichever structure determination technique is used. It is very important to collect the most accurate data possible: counting statistics must be carefully examined and the preferred orientation should be overcome as much as possible since experience shows that data suffering from texture are more difficult to handle and the structure determination requires more effort because the extracted intensities are not reliable. In the present work, two data sets were collected at room temperature (T = 293 K): one with a Guinier camera (λ = 1.54056 Å) and the other at the synchrotron facility in Grenoble (ESRF, Swiss–Norwegian CGR beamline BM1B, λ = 0.99452 Å).

The compound under investigation shows an interesting spin-transition behaviour as a function of temperature (Fig. 1). The ground state of octahedral iron(II) is the low-spin (LS) state $^1A_1$ (S = 0). When the ligand field splitting (10 Dq or Δ) is small, the energy loss for filling the high-energy levels is smaller than the gain by breaking the electron pairs and the ions will be in the high-spin (HS) state (S = 2). Spin-transition complexes are compounds in which the difference between high spin and low spin can be overcome by thermal energy. At low temperature, the compound is in the low-spin state. When the temperature is raised, the energy of the system increases and the electrons switch to the high-spin state. The temperature at which the transition occurs depends on the ligand field of Fe^{II}.

Thermal spin crossover in coordination compounds of 3*d* transition metals has been well known for many years. The high-spin ($^5T_2$) to low-spin ($^1A_1$) crossover of octahedrally coordinated iron(II) can be investigated by a number of physical methods (Gütlich, 1981; Gütlich & Hauser, 1990).

Spin-crossover compounds of the form [Fe(alkyltetrazole)$_6$](X)$_2$ (with X = BF_4, ClO_4 or CF_3SO_3) were first described by Franke (Franke *et al.*, 1982). Systems of this type can undergo a spin transition of either 100% (Jeftic *et al.*, 1997; Wiehl, 1993), 67% (Hinek *et al.*, 1996), 50% (Wiehl, 1993) or 33% (Gütlich & Poganiuch, 1991; Stassen *et al.*, 2001) depending on the counterion and the substituent on the tetrazole ring. The switch in spin state (LS $\rightarrow$ HS) is accompanied by an increase of the Fe—N bond length (~1.99–2.16 Å) and has been explained by two electrons moving from a non-bonding orbital to an anti-bonding orbital. When the alkyltetrazole is 1-(2-chloroethyl)tetrazole (teec) and X = BF_4^-, two different spin transitions occur. The first one is centred around 107.5 K and a second one around 190 K (Fig. 1). Both transitions probably involve 50% of the Fe^{II} ions and are reversible. Also, *d–d* excitations alter and a change in colour (red/purple in the case of low spin to white in the case of high spin) can be observed.

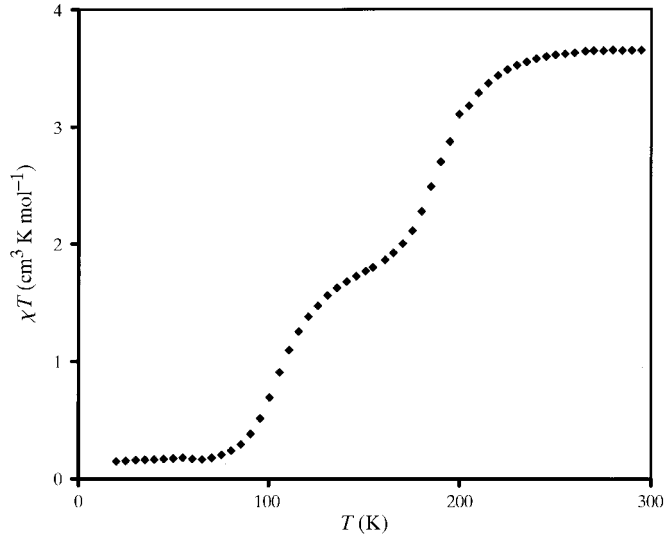

Figure 1
Spin transitions in Fe(teec)$_6$(BF$_4$)$_2$. Variation of the magnetic susceptibility (χT) as a function of the temperature (T) (Stassen *et al.*, 2001).

As yet, there are two possible explanations for this phenomenon. The first one is the occurrence of an extra thermodynamical stabilization when 50% of the Fe^{II} ions are in the high-spin state and 50% in the low-spin state, as suggested by the plateau at T = ~160 K in Fig. 1. A second possibility is that two different Fe^{II} ions are present in the system, each possessing a different thermal spin-state switching and thus in principle distinguishable by ^{57}Fe Mössbauer spectroscopy (Garcia *et al.*, 1999). From the ^{57}Fe Mössbauer experiments carried out no definite conclusion could be drawn and a crystal structure determination was undertaken.

2. Materials and methods

2.1. Chemical preparation

1-(2-Chloroethyl)tetrazole (teec) has been obtained by refluxing 1 mol of 1-chloroethylamine hydrochloride and 1 mol of sodium azide in 400 ml of acetic acid and 700 ml of triethylorthoformate for 3 h. After evaporation of the excess reagents and solvent, and removing the formed salts by filtration, teec crystallizes in 2-propanol after several hours as white blocks. Yield 70%. Elemental analysis: found (calc.): C, 27.3 (27.2); H, 4.0 (3.8); N, 42.4 (42.3)%. ^{1}H NMR (p.p.m.): 9.46 (s, H5), 4.85 (t 5.58 Hz, CH_2), 4.10 (t 5.58 Hz, CH_2Cl). ^{13}C NMR (p.p.m.): 144.4 (C5), 49.2 (C6), 42.8 (C7).

[Fe(teec)$_6$](BF$_4$)$_2$ has been formed by dissolving 1 mmol of Fe(BF$_4$)$_2$·4H$_2$O and 6 mmol of teec in 50 ml of ethanol. The complex formed as a white polycrystalline precipitate. Elemental analysis: found (calc.): C, 21.8 (21.1); H, 3.1 (3.0); N, 32.4 (32.8)%.

2.2. Sample preparation and data collection

The first data set of this compound was collected using an FR 552 Guinier–Johansson camera (Nonius, Delft, The Netherlands) equipped with a Johansson monochromator using Cu $K\alpha_1$ radiation (λ = 1.54056 Å). The samples were prepared by slightly pressing the powder into a thin layer on Mylar foil. To improve particle statistics the sample holder was rotated in the specimen plane. For indexing of the patterns accurate positions of as many lines as possible were collected by reading out the Guinier photographs with an optical

instrument. Using a Johansson LS-18 microdensitometer the Guinier photographs were digitized from 4.0 to 81° 2θ in steps of 0.01° 2θ.

The second data set was taken at the European Synchrotron Radiation Facility (2001*a*; ESRF, Grenoble, France), at the Swiss–Norwegian CRG beamline (SNBL) BM1B, with λ = 0.99542 Å. A two-circle diffractometer is available at the SNBL for high-resolution powder-diffraction measurements (European Synchrotron Radiation Facility, 2001*b*). The diffractometer is equipped with four parallel detectors, so four complete patterns are collected simultaneously, with offsets in 2θ of 1.1°. A Si-111 analyser crystal is mounted in front of each detector (NaI scintillation counter), resulting in an intrinsic resolution (FWHM) of approximately 0.01° 2θ at a wavelength of 1 Å. The sample was prepared into a capillary of 0.5 mm diameter and rotated during the measurement. Data were taken by continuous scanning in the interval $3.04 < 2\theta < 54°$. Taking into account the increase of reciprocal lattice point density with 2θ and to mimic a single-crystal-like data collection, special 2θ scan protocols were devised in order to expose each reciprocal lattice point to an approximate equal amount of radiation. Finally the data were binned at 0.005° 2θ.

2.3. Structure solution and refinement

The Guinier powder-diffraction pattern was indexed using the program *ITO* (Visser, 1969). Both Guinier and synchrotron powder-diffraction patterns were decomposed with the full-pattern decomposition (FPD) program *MRIA* (Zlokazov & Chernyshev, 1992) using a split-type pseudo-Voigt profile function (Toraya, 1986) into X_{obs} values (for the definition of X_{obs} values see Chernyshev & Schenk, 1998). The background was fitted with a fifth-order polynomial, cell parameters were refined and zero correction was applied.

2.3.1. Grid search. Taking into account the space group ($P2_1/c$) and volume requirements (Z = 2), the molecule was assumed to be centrosymmetric and with the metal kept fixed in a special position (0,0,0 was used), only half of the molecule was required as a search model. The initial search model was taken from the work of Wiehl (1993), having as a refcode JANSAS01 in the Cambridge Structure Database (Allen & Kennard, 1993) and modified using the program *XTAL*3.7 (Hall *et al.*, 2000) to give the desired model. To obtain this model the last $-CH_3$ group of the propyltetrazole was replaced by Cl at a distance of 1.79 Å. The grid-search procedure was split into the following searches:

(i) a rotational search to position the $(teec)_3$ moiety,

(ii) a translational/rotational search to locate BF_4^- and

(iii) a torsion-angle search to optimize the orientation of the tetrazole rings and the chloroethyls.

The rotational search of the $(teec)_3$ moiety was always carried out using 80 low-angle X_{obs} values and an initial rotation step of 10° in the whole angular range (φ = 0–180°, ψ = 0–180°, κ = 0–360°). In order to locate more precisely a minimum, the steps were gradually reduced to 1° and additional searches were carried out until the position was established.

Table 1
FPD results for Guinier (λ = 154056 Å) and FPD/RR results for synchrotron (λ = 099542 Å) data.

	Guinier data	Synchrotron data	
	FPD	FPD	RR
2θ range (°)	4–44	3.04–28.54	3.04–45.04
Resolution (Å)	2.06	2.02	1.08
Rp	0.0302	0.0610	0.0689
wR	0.0407	0.0719	0.0805
GoF	0.0200	0.0109	0.0138
a (Å)	12.2013 (15)	12.1977 (7)	12.1966 (11)
b (Å)	17.9994 (13)	17.9693 (9)	17.9677 (13)
c (Å)	10.5832 (8)	10.5668 (5)	10.5667 (8)
β (°)	90.560 (6)	90.548 (4)	90.555 (5)
V (Å)^3	2324.1 (4)	2316.0 (3)	2315.5 (3)

The search for BF_4^- was carried out with 80 low-angle X_{obs} values by applying in the beginning only translations with a step of 0.5 Å within a quarter of the cell. After having located an approximate position, rotations were applied as well with a step of 10° within the whole angular range. Finally, the search was restricted to a smaller area with a translation step of 0.1 Å and a rotational step of 1°.

A torsion-angle search exploiting 150 X_{obs} values was applied to determine more accurately the position of the rings and the chloroethyl side chains, as shown in Fig. 2. The torsion angles *t*1, *t*2 and *t*3 were varied simultaneously for each of the three teec ligands in steps of 20° in the beginning, but at the end the step was reduced to 1°. The procedure was carried out by means of a script, which varied systematically the relevant torsion angles and created automatically a new input for the grid-search procedure in the *MRIA* program. Afterwards, step (ii) was repeated in order to locate more precisely BF_4^-.

An alternative, applying first a torsion-angle variation before searching for the BF_4^-, has also been carried out, but after completing the grid search the structural models were almost the same, so this line was not pursued any further.

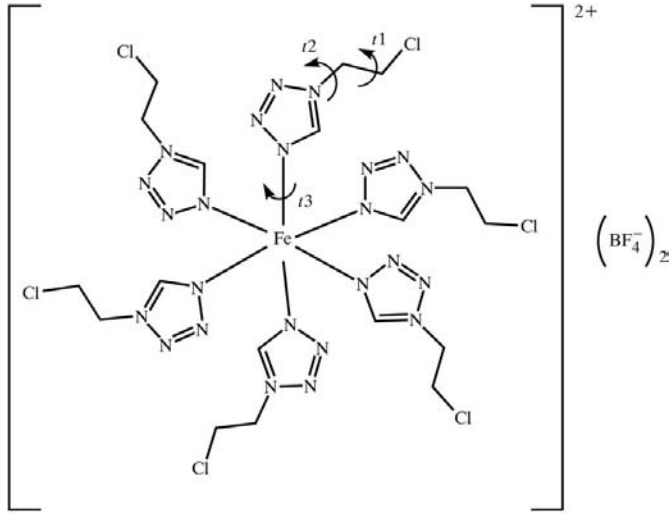

Figure 2
Chemical diagram of $F(teec)_6(BF_4)_2$ showing the systematic torsion-angle parameters (*t*1, *t*2 and *t*3), as used for each of the teec ligands.

Independently of the order of the steps followed, it is useful to repeat the second step at the end in order to optimize the position of the fragments. In this case, the step order followed was (i)–(ii)–(iii)–(ii).

2.3.2. Rietveld refinement. A Rietveld refinement (RR) procedure was carried out with synchrotron data. The background parameters were refined (fifth-order polynomial), a split-type pseudo-Voigt profile (Toraya, 1986) was assigned to the reflections and texture correction was applied using the symmetrized-harmonics expansion method (Ahtee *et al.*, 1989; Järvinen, 1993). Zero correction and cell-parameter refinement were applied as well.

In order to avoid distortion of the fragments a distance-restrained refinement as described by Baerlocher (1993) was applied to intramolecular distances (< 6 Å) with $\sigma = 1\%$ of the ideal distance. The weight c_w (Baerlocher, 1993, p. 188) that weighs the residual function of the distance restraints S_R *versus* the Rietveld residual function S_Y was gradually reduced from 27.7 to 3.2. Trials to lower c_w further resulted in a distortion of the model. The coordinates of both B and F of BF_4^- were refined in the beginning, but kept fixed afterwards. Atomic displacement parameters of Fe and Cl could be refined isotropically to $U_{eq} = 0.049$ (8) for Fe and 0.135 (8) Å^2 for Cl. Attempts to refine the atomic displacement parameters of N and C were not successful and therefore they were kept fixed, as well as the atomic displacement parameters of B, F and H, at 0.05 Å^2.

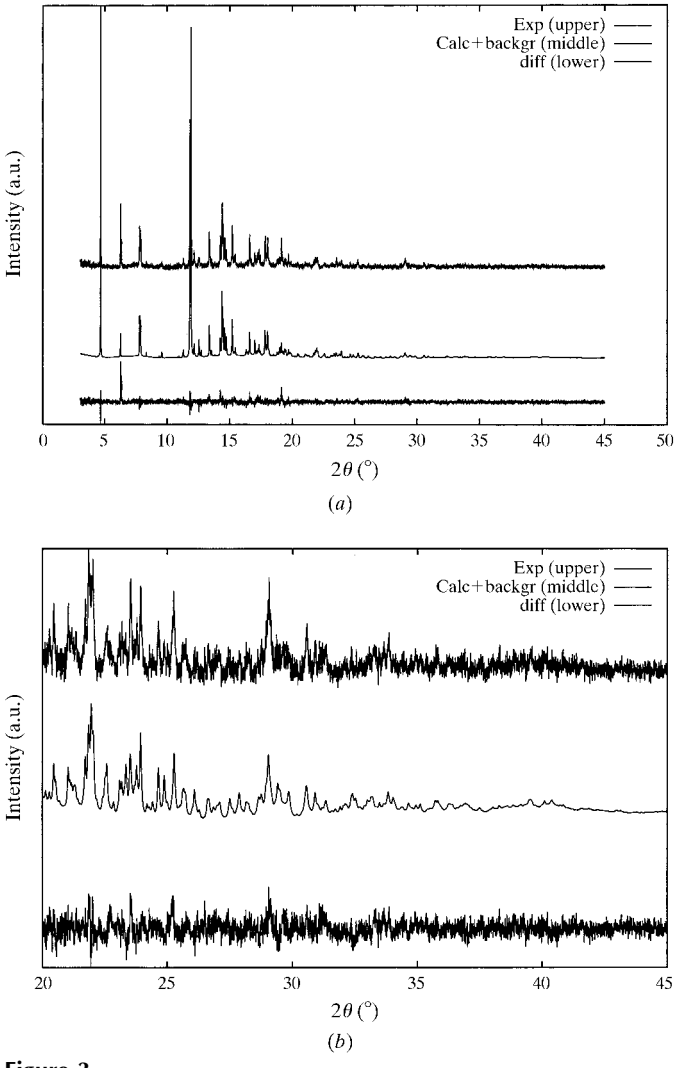

Figure 3
(*a*) Synchrotron powder diffraction pattern (λ = 0.99542 Å) of $[Fe(teec)_6(BF_4)_2]$ (upper), as calculated from the refined crystal structure (middle) and difference between these patterns (lower), and (*b*) with $20 < 2\theta < 45°$.

Table 2
Texture correction and peak-profile parameters with their standard uncertainties as calculated after Rietveld refinement.

Texture correction parameters	Value	Peak profile parameters	Value
*Y*20	−0.30 (5)	*rl*1	−0.08 (9)
*Y*22	−0.73 (4)	*rl*2	4.9 (6)
Y-22	0.33 (5)	*rl*3	0.012 (5)
*Y*40	0.64 (7)	*rh*1	−0.73 (9)
*Y*42	−0.17 (4)	*rh*2	5.6 (6)
Y-42	1.23 (6)	*rh*3	0.095 (4)
*Y*44	0.37 (4)	*a*1	0.82 (7)
Y-44	0.16 (6)	*a*2	0.060 (10)
*Y*60	0.92 (7)	*a*3	−0.0079 (6)
*Y*62	−0.03 (4)	*U*	0.126 (10)
Y-62	0.69 (6)	*V*	0.0035 (13)
*Y*64	0.76 (4)	*W*	0.00007 (5)
Y-64	−0.02 (4)		
*Y*66	0.14 (4)		
Y-66	0.09 (3)		

3. Results and discussion

The unit cell resulting after indexing the Guinier pattern was monoclinic with $a = 12.22$, $b = 18.02$, $c = 10.60$ Å and $\beta = 90.51°$ and was used as a starting point for the FPD of both the Guinier and synchrotron patterns. On the basis of the systematic extinctions, $P2_1/c$ was assumed to be the most likely space group and $Z = 2$ in view of a density of ∼1.43 g cm^{-3} for this type of material (Wiehl, 1993). Unit-cell parameters and the results of the FPD and RR (synchrotron only) are listed in Table 1.[1] Texture correction parameters and the peak-profile parameters are listed in Table 2. The final RR fit between the calculated and the experimental synchrotron XRPD pattern is shown in Fig. 3.

3.1. Methodology

For methodological reasons the grid search was carried out using extracted X_{obs} values from both Guinier and synchrotron data. Although the FPD delivered 200 (Guinier data) and 220 (synchrotron data) X_{obs} values, for the initial grid search only the 80 lowest resolution X_{obs} values were used, which corresponded to 67 separate and 28 overlapping reflections in the case of Guinier data, and 68 separate and 25 overlapping reflections in the case of synchrotron data. A number of minima was found with approximately the same $R(X_{obs})$. The

[1] Supplementary data for this paper are available from the IUCr electronic archives (Reference: NA0120). Services for accessing these data are described at the back of the journal.

Table 3
$R(X)$ and positions of the moieties after every step of the grid search.

φ, ψ and κ are the rotational angles, x, y and z the translational parameters, and $t1$, $t2$ and $t3$ the torsion angles, as shown in Fig. 2.

Positional parameters	Grid search φ, ψ, κ (°)	Search for BF_4^-, $Fe(teec)_6^{2+}$ is imported φ, ψ, κ (°) x, y, z (Å)	Torsion variation (TV) φ, ψ, κ $t1$, $t2$, $t3$ (°)	Search BF_4^- and $Fe(teec)_6^{2+}$ after TV φ, ψ, κ (°) x, y, z (Å)
Guinier				
Position	139, 159, 267	81, 35, 204 0.000, 0.161, 0.500	0, 0, −1 −125, −119, −137	141, 114, 111 0.0, 0.830, 0.507
$R(X)$	0.758	0.553	0.427	0.416
Synchrotron				
Position	139, 159, 267	41, 25, 222 0.000, 0.152, 0.500	0, 0, 0.5 +344, −3, +3	44, 27, 223 0.000, 156, 500
$R(X)$	0.778	0.457	0.391	0.390

models corresponding to these minima were plotted with the program *PLUVA* v3.0 (Driessen *et al.*, 1988) and could be reduced finally to the same model because of the internal symmetry of the molecule. Besides the centre of symmetry the ligands can be arranged in several equivalent conformations. The first part of the grid search led to the same minimum for Guinier and synchrotron data (Table 3).

In the second part of the grid search, BF_4^- was finally located at approximately the same position with either of the two data sets (Table 3). The rotational search led to several equivalent minima, which was expected because of the internal symmetry of BF_4^- and its well known disorder with F positions being not fully occupied (Wiehl, 1993; Hinek *et al.*, 1996; Stassen *et al.*, 2000). After plotting with the program *PLUVA*, it turned out that all of them could be reduced to a small number of models and finally one of them was chosen.

A torsion-angle variation was carried out in order to determine more accurately the orientation of the ligands. The search with Guinier data led to a quite distinct minimum (referred hereafter as Model 1), while the search with synchrotron data led to two very close minima [$R(X)$ = 0.397 and 0.399], the first one being the same as Model 1 and the second being referred to hereafter as Model 2. After an analysis of the packing of the structures Model 1 was considered less likely than Model 2 and therefore a more detailed torsion-angle variation was carried out using more (100, 120, 150 and 172) X_{obs} values. For Guinier data the increase of the number of reflections led only to the decrease of the difference in $R(X)$ between Model 1 and Model 2, but the minima remained the same. In the case of synchrotron data with 100–150 X_{obs} values, the two minima corresponding to Model 1 and Model 2 were clearly distinct with Model 2 having the lowest $R(X)$ value. When using 172 X_{obs} values, the difference between the $R(X)$ values corresponding to these two minima became smaller. Finally the solution found with 150 X_{obs} values was chosen as a starting model for the RR. From the above it can be concluded that the number of X_{obs} values to be used should not be very small because a torsion-angle variation is quite detailed and requires more information, but should also not be too large since the high-angle reflections are less reliable due to the severe overlap.

After torsion-angle variation, BF_4^- was again searched for to improve its position, but there was no change of its initial position. Using the final model of the grid search, the structure was subsequently refined using the Rietveld module in the program *MRIA*.

In Table 3, for both data sets, $R(X)$ values and the positions of the moieties after every step of the grid search are given for the case of 80 X_{obs} values, showing the change in $R(X)$ at the distinct stages of the grid search. A remarkable drop in $R(X)$ occurs after positioning BF_4^- with both Guinier and synchrotron data. Torsion-angle variation also significantly improved the model.

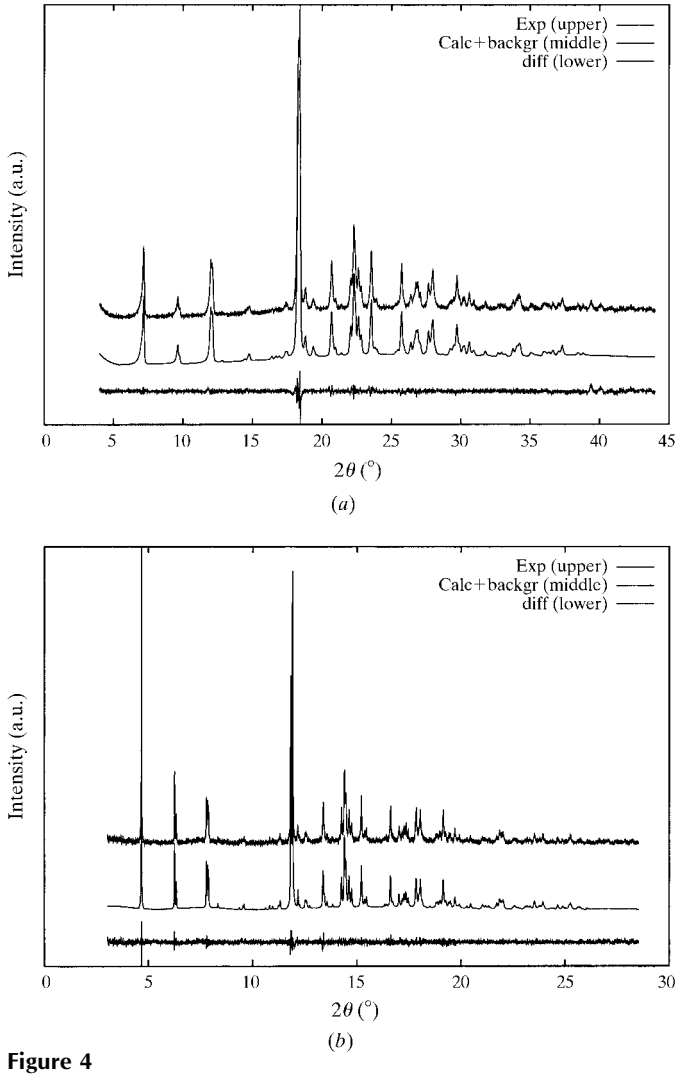

Figure 4
Diffraction patterns of (*a*) Guinier and (*b*) synchrotron data after the FPD showing the preferred orientation problem encountered during the data collection.

The fact that with Guinier data the torsion-angle search led to a different solution may have several explanations. From the fit between experimental and calculated XRPD patterns after FPD, shown in Fig. 4, it is clear that there is good agreement in the positions of the reflections found after FPD, but not in the values of the intensities. The data suffer from preferred orientation as can be seen from the difference in the intensities, especially at the low-angle range. Therefore, differences in the grid-search results can be expected. Furthermore, the Guinier-data intensities are measured as optical densities and then converted to X-ray intensities, which also reduces the quality of the data. Both data sets were adequate to position an approximate structural model, but for a more demanding search, such as the torsion variation, high-quality synchrotron data were necessary.

The experimental synchrotron pattern seems to be quite 'noisy' and peak shapes are abnormal with a shoulder-like behaviour and characteristic zigzag pattern (Fig. 5). A major reason for this seems to be a particle statistics problem. In order to avoid absorption a narrow capillary (diameter of 0.5 mm) was used, but because of the relatively large needle-shape particles the capillary probably was not packed in an optimum way. Spinning of the sample improved slightly the particle statistics, but did not correct the problem sufficiently, as can be observed in Fig. 5. Obviously, a smooth profile shape is not adequate to describe these peaks and therefore a 'noisy' difference pattern results.

Preferred orientation is likely to be an additional reason for the bad particle statistics in some directions, because the needle-like shape of the crystallites favour a longitudinal arrangement of the crystallites. A texture correction was applied and led to a significant improvement of the fit.

3.2. Crystal structure description

The Fe in the centrosymmetric $Fe(teec)_6^{2+}$ complex is at a special position and is almost perfectly octahedrally coordinated by the neighbouring N atoms at the distances 2.201 (16)–2.220 (16) Å. All N—Fe—N angles show almost ideal octahedral symmetry with a maximum deviation of 0.8° from 90° (all distances and angles given in the text have been calculated with the program *PLATON*; Spek, 2001). The four in-plane N atoms form an almost perfect square (deviation smaller than 1° from 90°). The structure forms layers along the *b* and *c* axes, perpendicular to the *a* axis (Figs. 6*a* and *b*), and within the layers the Fe and B atoms exhibit a pseudo-trigonal symmetry (Fig. 7). All figures displaying the structure have

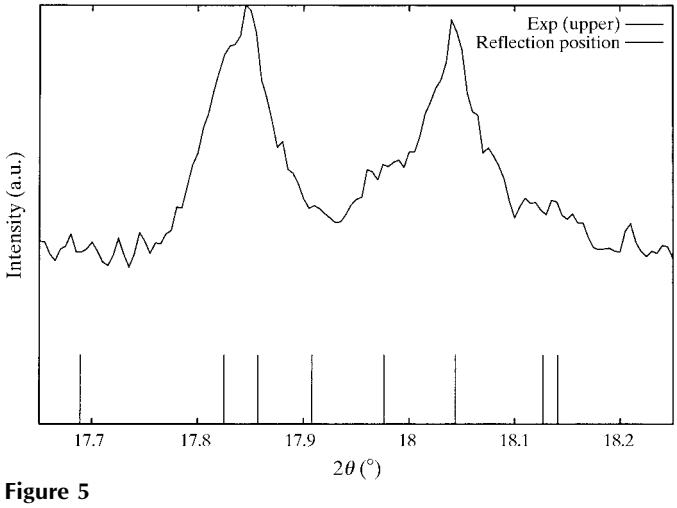

Figure 5
Excerpt of the synchrotron powder diffraction pattern showing the peak shapes affected by counting statistics. The small vertical lines at the 2θ axis indicate the calculated positions of the reflections.

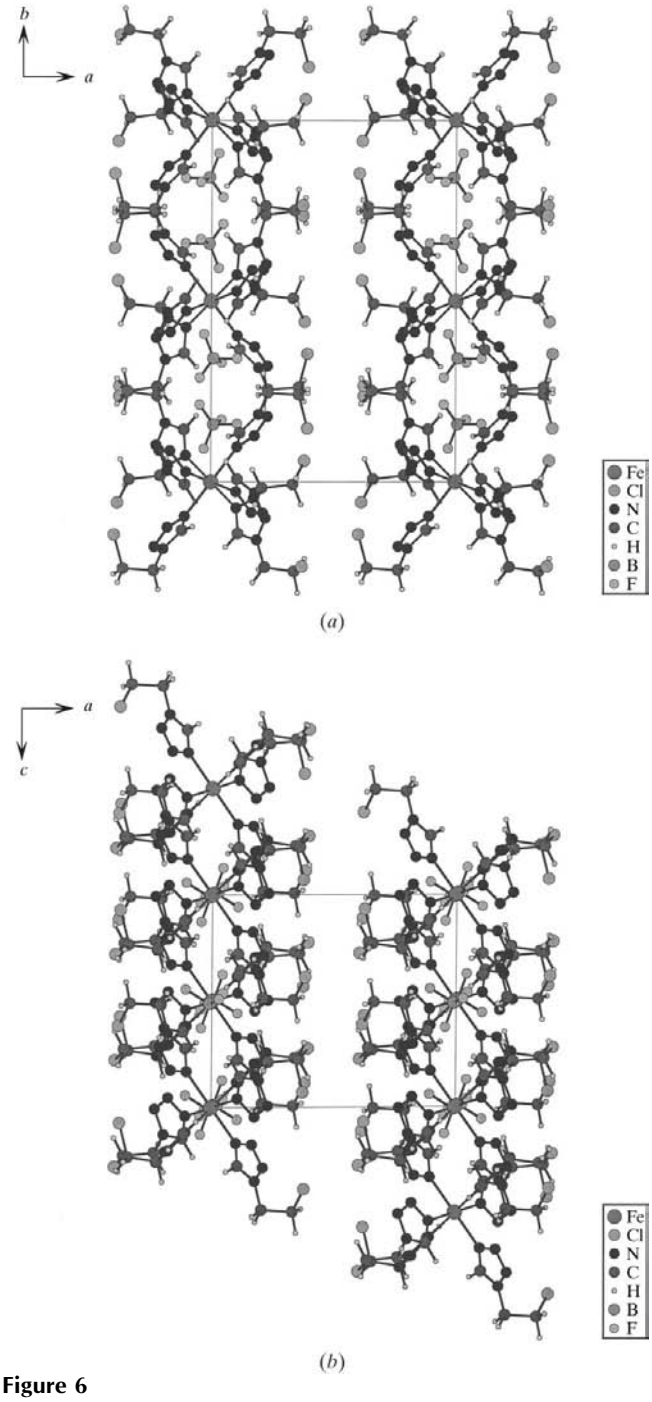

Figure 6
The structure forms layers along (*a*) the *b* axis and (*b*) the *c* axis, perpendicular to the *a* axis

been made with the program *DIAMOND* (Pennington, 1999; Cordier, 1999).

The BF_4^- moieties are arranged in these electrically neutral layers and on the same planes as Fe at $x = 0$. The distances between neighbouring B atoms are around 6 Å. Typical Fe—B distances range from 5.9 to 6.14 Å. All Fe are lying on the twofold axis.

Each tetrazole ring is planar and the atoms directly bonded to a tetrazole ring (Fe and C2) also lie in that plane with a maximum deviation from the plane of 0.10 (3) Å. Angles between these planes and the *bc* plane range from 45.0 (9) to 49.3 (10)°. Dihedral angles between the tetrazole planes are around 73° (±2). Each tetrazole plane is almost perpendicular to the plane determined by Fe and the two N atoms connected to the other two tetrazole rings.

B atoms lie at the centre of almost spherical cavities (average radius of 3.1 Å) formed by the neighbouring H atoms. There are no classical hydrogen bonds between donors and acceptors.

The molecular structure is shown in Fig. 8. The non-H atoms of the asymmetric unit are labelled.

The structure is very similar to the structure of $[Fe(mtz)_6](BF_4)_2$ (mtz = methyltetrazole) described in the work of Wiehl (1993). Both structures are monoclinic and the cation complex is centrosymmetric as well. The structures are layered with Fe and B exhibiting pseudo-trigonal symmetry within the layers following the general feature of the series $[Fe(Rtz)_6(BF_4)_2$ (Hinek *et al.*, 1996) and Fe—B distances being about the same. However, the two structures show a different spin-crossover behaviour since the teec compound exhibits a two-step spin crossover, but the mtz compound only a single-step spin crossover of 50% of the Fe^{II} ions. At this moment the exact mechanism of the two-step spin transition of $Fe(teec)_6(BF_4)_2$ is not clear. In view of the space-group requirements with $Z = 2$ and the Fe being on the same special position, there is no evidence that the Fe atoms are behaving differently. Therefore, the two-step spin crossover cannot be attributed to the existence of two differently behaving Fe^{II} ions, as in the case of $[Fe(mtz)_6]X_2$, $X = BF_4$ or ClO_4 (Wiehl, 1993) and $[Fe(etz)_6](BF_4)$ (Hinek *et al.*, 1996), where two different sites for Fe^{II} ions were assumed on the basis of Mössbauer measurements and confirmed by single-crystal structure analysis.

This leaves the option that in the case of $[Fe(teec)_6](BF_4)_2$ at lower temperature a phase transition takes place, as also happens in the case of $[Fe(ptz)_6]X_2$ (X as above; Wiehl, 1993), which leads to independent Fe^{II} ion sites and gives rise to a HS–LS spin crossover. The plateau observed (Fig. 1) at $T \simeq 160$ K could be due to an extra thermodynamical stability with 50% of the Fe^{II} ions being in the high-spin state and 50% in the low-spin state. In order to give a definite answer to this hypothesis, X-ray (powder) diffraction experiments at lower temperatures should be carried out.

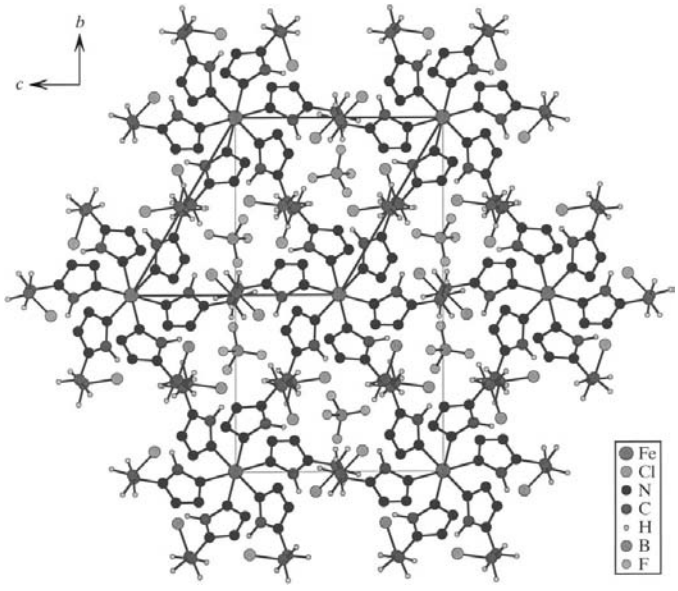

Figure 7
View along the *a* axis; within these layers the Fe and B atoms exhibit a pseudo-trigonal symmetry, shown with a thick line.

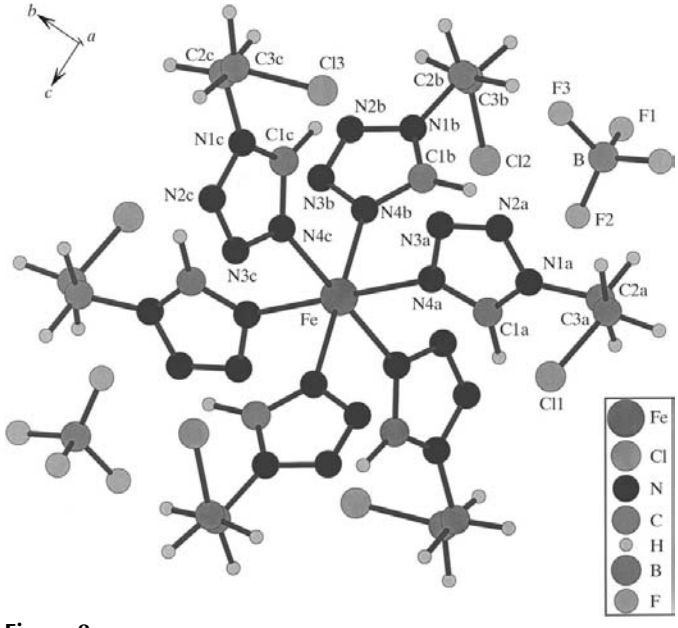

Figure 8
Molecular crystal structure of $[Fe(teec)_6^{2+}](BF_4)_2$ showing the numbering scheme.

The authors would like to thank the ESRF (Grenoble, France) for the opportunity to perform the synchrotron diffraction experiments and especially Drs Wouter van Beek and Hermann Emerich for their invaluable help at the beamline BM1B Swiss–Norwegian CRG (SNBL).

References

Ahtee, M., Nurmela, M., Suortti, P. & Järvinen, M. (1989). *J. Appl. Cryst.* **22**, 261–268.
Allen, F. H. & Kennard, O. (1993). *Chem. Des. Autom. News*, **8**, 31–37.
Baerlocher, C. (1993). *The Rietveld Method*, edited by R. A. Young, pp. 187–196. Oxford University Press.
Cheary, R. W. & Coelho, A. (1992). *J. Appl. Cryst.* **25**, 109–121.

Chernyshev, V. V. & Schenk, H. (1998). *Z. Kristallogr.* **213**, 1–3.
Cordier, G. (1999). *Nachr. Chem. Techn. Lab.* **47**, 1437–1438.
Driessen, R. A. J., Loopstra, B. O., Bruijn de, D. P., Kuipers, H. P. C. E. & Schenk, H. (1988). *J. Comput.-Aided Mol. Des.* **2**, 225–233.
European Synchrotron Radiation Facility (2001*a*). *BM1B.* http://www.esrf.Fr/exp_facilities/BM1A/DescriptionB.htm.
European Synchrotron Radiation Facility (2001*b*). Powder diffraction setup at SNBL. http://www.esrf.Fr/exp_facilities/BM1A/powder.htm.
Franke, P. L., Haasnoot, J. G. & Zuur, A. P. (1982). *Inorg. Chim. Acta*, **59**, 5–9.
Garcia, Y., Kahn, O., Rabardel, L., Chansou, B., Salmon, L. & Tuchagues, J. P. (1999). *Inorg. Chem.* **38**, 4663–4670.
Giacovazzo, C. (1996). *Acta Cryst.* A**52**, 331–339.
Goubitz, K., Čapková, P., Melánová, K., Molleman, W. & Schenk, H. (2001). *Acta Cryst.* B**57**, 178–183.
Goubitz, K., Sonneveld, E. J., Chernyshev, V. V., Yatsenko, A. V., Zhukov, S. G., Reiss, C. A. & Schenk, H. (1999). *Z. Kristallogr.* **214**, 469–474.
Gütlich, P. (1981). *Structure and Bonding*, edited by M. J. Clarke, P. Hemmerich, J. B. Goodenough, J. A. Ibers, C. K. Jørgensen, J. B. Neilands, D. Reiden, R. Weiss & R. J. P. Williams, Vol. 44, pp. 83–196. Berlin: Springer Verlag.
Gütlich, P. & Hauser, A. (1990). *Coord. Chem. Rev.* **97**, 1–22.
Gütlich, P. & Poganiuch, P. (1991). *Angew. Chem. Int. Ed. Engl.* **30**, 975–977.
Hall, S. R., du Boulay, D. J. & Olthof-Hazekamp, R. (2000). Editors. *XTAL*3.7. University of Western Australia, Lamb, Perth.
Helmholdt, R. B., Sonneveld, E. J. & Schenk, H. (1998). *Z. Kristallogr.* **213**, 596–598.
Hinek, R., Spiering, H., Schollmeyer, D., Gütlich, P. & Hauser, A. (1996). *Chem. Eur. J.* **2**, 1427–1434.
Jansen, J., Peschar, R. & Schenk, H. (1992*a*). *J. Appl. Cryst.* **25**, 231–236.
Jansen, J., Peschar, R. & Schenk, H. (1992*b*) *J. Appl. Cryst.* **25**, 237–243.
Jansen, J., Peschar, R. & Schenk, H. (1993). *Z. Kristallogr.* **206**, 33–43.
Järvinen, M. (1993). *J. Appl. Cryst.* **26**, 525–531.
Jeftic, J., Hinek, R., Capelli, S. C. & Hauser, A. (1997). *Inorg. Chem.* pp. 3080–3087.
Langevelde, A. J. van, Capková, P., Sonneveld, E. J., Schenk, H., Trchova, M. & Ilavsky, M. (1999). *J. Synchrotron Rad.* **6**, 1035–1043.
Louër, D. (1998). *Acta Cryst.* A**54**, 922–933.
McCusker, L. B., Von Dreele, R. B., Cox, D. E., Louër, D. & Scardi, P. (1999). *J. Appl. Cryst.* **32**, 36–50.
Pennington, W. T. (1999). *J. Appl. Cryst.* **32**, 1028–1029.
Spek, A. L. (2001). *PLATON.* Utrecht University, The Netherlands.
Stassen, A. F., Dova, E., Ensling, J., Gutlich, P., Haasnoot, J. P., Reedijk, J. & Schenk, H. (2001). To be published.
Stassen, A. F., Roubeau, O., Ferrero Gramage, I., Linares, J., Varret, F., Mutikainen, I., Turpeinen, U., Haasnoot, J. G. & Reedijk, J. (2001). *Polyhedron*, **20**, 1699–1707.
Stassen, A. F., de Vos, M., van Koningsbruggen, P. J., Renz, F., Ensling, J., Kooijman, H., Spek, A. L., Haasnoot, J. G., Gutlich, P. & Reedijk, J. (2000). *Eur. J. Inorg. Chem.* pp. 2231–2237.
Toraya, H. (1986). *J. Appl. Cryst.* **19**, 440–447.
Visser, J. W. (1969). *J. Appl. Cryst.* **2**, 89–95.
Wiehl, L. (1993). *Acta Cryst.* B**49**, 289–303.
Zlokazov, V. B. & Chernyshev, V. V. (1992). *J. Appl. Cryst.* **25**, 447–451.